BRAIN CONNECTIVITY
Volume 5, Number 7, 2015

DOI: 10.1089/brain.2014.0245

Quantitative Analysis of Myelin and Axonal Remodeling in the Uninjured Motor Network After Stroke

Ying-Chia Lin,[1] Alessandro Daducci,[2] Djalel Eddine Meskaldji,[3,4] Jean-Philippe Thiran,[2] Patrik Michel,[5] Reto Meuli,[6] Gunnar Krueger,[7,8] Gloria Menegaz,[1] and Cristina Granziera[2,8,9]

Abstract

Contralesional brain connectivity plasticity was previously reported after stroke. This study aims at disentangling the biological mechanisms underlying connectivity plasticity in the uninjured motor network after an ischemic lesion. In particular, we measured generalized fractional anisotropy (GFA) and magnetization transfer ratio (MTR) to assess whether poststroke connectivity remodeling depends on axonal and/or myelin changes. Diffusion-spectrum imaging and magnetization transfer MRI at 3T were performed in 10 patients in acute phase, at 1 and 6 months after stroke, which was affecting motor cortical and/or subcortical areas. Ten age- and gender-matched healthy volunteers were scanned 1 month apart for longitudinal comparison. Clinical assessment was also performed in patients prior to magnetic resonance imaging (MRI). In the contralesional hemisphere, average measures and tract-based quantitative analysis of GFA and MTR were performed to assess axonal integrity and myelination along motor connections as well as their variations in time. Mean and tract-based measures of MTR and GFA showed significant changes in a number of contralesional motor connections, confirming both axonal and myelin plasticity in our cohort of patients. Moreover, density-derived features (peak height, standard deviation, and skewness) of GFA and MTR along the tracts showed additional correlation with clinical scores than mean values. These findings reveal the interplay between contralateral myelin and axonal remodeling after stroke.

Key words: diffusion-spectrum imaging; graph; longitudinal study; magnetization transfer ratio; stroke

Introduction

Connectivity remodeling after stroke has been reported in both injured (Sotak, 2002) and uninjured hemispheres (Carmichael et al., 2001; Chollet et al., 1991; Granziera et al., 2007; Jones et al., 1996; Luke et al., 2004; Rehme et al., 2011; Riecker et al., 2010; Takatsuru et al., 2009; Weiller et al., 1992, 1993). Diffusion magnetic resonance imaging (dMRI) studies showed contralesional changes in scalar measures as mean fractional anisotropy (FA) and apparent diffusion coefficient (Granziera et al., 2012a, Ozsunar et al., 2004); on the other hand, tractography-based dMRI investigations revealed a variable increase or decrease in average number/density/probability of fiber trajectories (Crofts et al., 2011; Granziera et al., 2012b). Despite these average measures indicate the presence and the degree of contralesional axonal remodeling, they fail in providing detailed information about the nature of the underlying pathological process (i.e., myelin or axonal plasticity) (Alexander et al., 2007; Beaulieu, 2006).

The stroke injury is known to affect both axonal (Assaf and Pasternak, 2008; Pierpaoli and Basser, 1996) and myelin integrity (Assaf and Pasternak, 2008; Kinnunen et al., 2010; Pierpaoli and Basser, 1996; Wang et al., 2012) through oxidative damage and plastic remodeling following

[1]Department of Computer Science, University of Verona, Verona, Italy.
[2]STI/IEL/LTS5, Ecole Polytechnique Fédérale de Lausanne, Lausanne, Switzerland.
[3]Institute of Bioengineering, Ecole Polytechnique Fédérale de Lausanne (EPFL), Lausanne, Switzerland.
[4]Department of Radiology and Medical Informatics, University of Geneva, Geneva, Switzerland.
[5]Stroke Center, Department of Clinical Neurosciences, Centre Hospitalier Universitaire Vaudois, University of Lausanne, Lausanne, Switzerland.
[6]Department of Radiology, Centre Hospitalier Universitaire Vaudois, University of Lausanne, Lausanne, Switzerland.
[7]Healthcare Sector IM&WS S, Siemens Schweiz AG, Lausanne, Switzerland.
[8]Advanced Clinical Imaging Technology Group, Ecole Polytechnique Fédérale de Lausanne, Lausanne, Switzerland.
[9]Laboratoire de Recherche en Neuroimagerie and Neuroimmunology Unit, Department of Clinical Neurosciences, Centre Hospitalier Universitaire Vaudois and University of Lausanne, Lausanne, Switzerland.

the acute event might show variable degree of sprouting/axonal degeneration and de/remyelination (Lin et al., 2013; van den Heuvel et al., 2010). Yet, despite the importance of myelin remodeling after stroke, little is known about poststroke myelin changes; in fact, only one study to date evidenced persistent myelin loss in both ipsi and contralesional hemispheres in chronic ischemic stroke patients (Borich et al., 2013).

In this work, we combined diffusion-spectrum imaging (DSI) (Wedeen et al., 2005) and magnetization transfer imaging (MTI) in order to investigate the substrate of contralesional motor connectivity remodeling after stroke.

Generalized fractional anisotropy (GFA) measures (Tuch, 2004), as obtained from DSI data, had been previously successfully exploited to provide evidence of plasticity in the uninjured motor network of stroke patients with motor deficits (Granziera et al., 2012b). As the studied motor network is mainly constituted by short cortico-cortical association connections and callosal fibers, the observed decrease in GFA suggests disruption or loss of the axonal structures and a GFA increase points at axonal sprouting or myelin growth. On the other hand, MTI supports with a semiquantitative measure of myelin integrity by means of the magnetization transfer ratio (MTR) (Henkelman et al., 2001); an increase in MTR indicates therefore an increase in myelination or loss of water and a decrease in MTR suggests myelin loss or increased water presence. The joint exploitation of GFA and MTR allows to establish to which extent myelin and pure axonal remodeling is responsible of the observed plasticity in the uninjured motor network after stroke. GFA and MTR are ''indirect'' quantitative metrics of structural integrity of the axon and its myelin sheet, derived from high-*b* value diffusion and magnetization transfer experiments (Ongur and Du, 2013). Various MRI-based metrics have been previously proposed to specifically quantify axonal and myelin integrity, such as radial and axonal diffusivity (Song et al., 2002, 2005; Sun et al., 2006), kurtosis characteristics (Farrell et al., 2010), and diffusion tensor spectroscopy combined to MTR (Ongur and Du, 2013). Our approach overcomes some limitations of previously proposed methods in regions of fiber crossing (axial and radial diffusivity [Wheeler-Kingshott and Cercignani, 2009]) and extends previous studies on q-space diffusion imaging data.

In this study, we performed (i) analysis by extracting the mean values of GFA and MTR in each connection between contralesional motor cortical areas (Chen et al., 2005; Gertheiss et al., 2013; van den Heuvel et al., 2010; Zhou et al., 2004) and (ii) density-derived feature analysis (Mandl et al., 2010; Nossin-Manor et al., 2013; Sled and Pike, 2001) of GFA and MTR histograms along a fiber tract. The final goal was to establish whether connectivity remodeling in the uninjured motor network depends mainly on axonal plasticity, myelin remodeling, or both.

Materials and Methods

Patient group

Ten stroke patients (6 men and 4 women [age = 60.3 ± 12.8 years, mean ± SD]) were enrolled in the study. Patients were admitted and treated at the Stroke Center of the Centre Hospitalier Universitaire Vaudois (CHUV) in Lausanne (Switzerland) and selected from the Acute STroke Registry and Analysis (ASTRAL) database (Michel et al., 2010). The inclusion criteria were (i) the presence of small- or medium-size stroke affecting the motor cortex and/or subcortical structures that are involved in motor control, (ii) the absence of previous stroke or other neurological, psychiatric, or systemic illnesses; and (iii) the absence of brainstem and cerebellar infarcts. Five patients benefitted from intravenous thrombolysis and all of them underwent standard rehabilitation programs (including physical and occupational therapy), as performed in CHUV. None used antidepressant or central nervous system stimulator drugs during rehabilitation. All subjects provided written informed consent prior to imaging and the Lausanne University Hospital review board approved the study protocol. All patients underwent three times DSI scans (i) within 1 week (tp1), (ii) 1 month (± 1 week, tp2), and (iii) 6 months (± 15 days, tp3) after stroke. Ten age- and gender-matched healthy controls were also included in the study (age = 56.1 ± 17.8 years, mean ± SD). Control group underwent two DSI scans a month apart (tp1c and tp2c).

Clinical assessment

Patients benefited of clinical assessment (NIHSS: National Institute of Health Stroke Scale; FIM: Functional Independence Measure; and RANKIN: modified Rankin scale scores) at each time point as reported (Granziera et al., 2012b). The motor part of NIHSS score (NIHSS motor) was derived from items 2 to 7 and 10 (www.nihstrokescale.org/) (Granziera et al., 2012b). Information on patient demographics and etiologic stroke mechanism (Ay et al., 2007) were obtained from medical records.

Imaging protocol

All DSI measurements (TR/TE = 6000/136 msec, FoV = $212 \times 212\,mm^2$, 34 slices, voxel = $2.2 \times 2.2 \times 3\,mm^3$ resolution, 257 diffusion directions, *b*-max = 8000 sec/mm^2, scan time = 25.8 min) were performed at 3T (Magnetom Trio a Tim System; Siemens, Erlangen, Germany) using a 32-channel head matrix coil as reported in Granziera and colleagues (2012b). MT scans were performed using a multiple-echo Fast Low Angle SHot (FLASH) sequence with (MT) and without (M0) magnetization transfer preparation (TR/TE = 48/8.25 msec, FoV = $256 \times 240\,mm^2$, voxel = $1 \times 1 \times 1.1\,mm^3$ resolution, 8 echos, scan time = 1.02 min × 2) as in the previous study (Helms et al., 2008). High-resolution MPRAGE images (TR/TE = 2300/3 msec, FoV = $256 \times 240\,mm^2$, voxel = $1 \times 1 \times 1.2\,mm^3$, scan time = 6.13 min) and T2-weighted images (TR/TE = 3000/84 msec, FoV = $448 \times 512\,mm^2$, voxel = $0.45 \times 0.45 \times 3\,mm^3$, scan time = 2.4 min) were acquired for anatomico-pathological reference. Total scan time was 36 min.

Image postprocessing

Segmentation of high-resolution MPRAGE images into the gray matter and white matter (including the cortical and subcortical regions) was performed using Freesurfer (www.surfer.nmr.mgh.harvard.edu). Primary (M1) and secondary motor regions (supplementary motor area [SMA], premotor ventral [PMv] area, and premotor dorsal [PMd] area) in the contralesional hemisphere were then identified using an atlas provided by the same software (84-region

parcellation). In the framework of the Connectome Mapping Toolkit (CMTK; www.cmtk.org) (Daducci et al., 2012; Gerhard et al., 2011), the orientation distribution functions (ODFs) were obtained using the Diffusion Toolkit (www.trackvis.org/dtk). Fiber tracking was performed by using the streamline-based algorithm (Granziera et al., 2012b) followed by the two major ODF directions (Daducci et al., 2012; Hagmann et al., 2007; Wedeen et al., 2008). Among motor areas, connections were divided into (i) intrahemispheric: fiber trajectories between couples of motor areas in the contralateral hemisphere and (ii) interhemispheric: each contralateral motor area and corpus callosum. Stroke lesion volumes were evaluated on MPRAGE images at tp3 using in-house software based on an implementation of the statistical parametric mapping (SPM) lesion segmentation toolbox for stroke lesions (www.fil.ion.ucl.ac.uk/spm/).

MTR was computed on the basis of two serially acquired images as (M0–MT)/M0, one with MT saturation (MT) and one without (M0), and GFA was calculated from diffusion data as in Granziera and colleagues (2012b). MTR maps were then registered to T2-weighted images and subsequently coregistered to the diffusion space ($b = 0$ sec/mm^2). FSL FLIRT command was used for linear (affine) image registration. All registrations were performed using FSL (www.fmrib.ox.ac.uk/fsl). Registration quality was checked by visual inspection.

Tract-based analysis, density-derived features, and motor network

Analysis was performed by calculating the mean GFA and MTR values along each tract and among all tracts connecting the motor regions of interest. GFA and MTR values were computed for each voxel and then averaged along each connection. Density-derived feature analysis was performed by computing histograms of MTR and GFA values along the tracts. Three density-derived features were extracted as in Figure 1 (standard deviation [SD], peak height, and skewness).

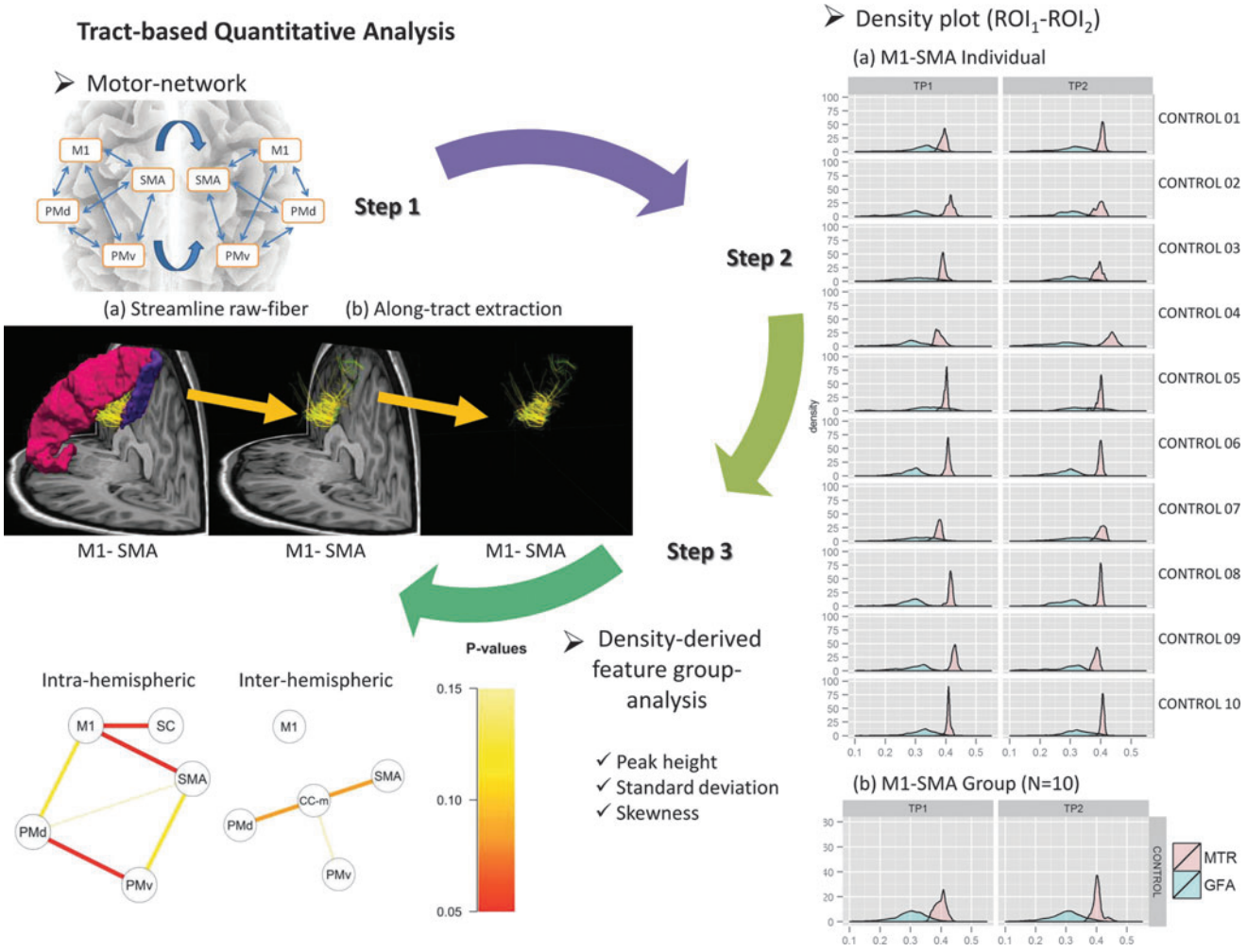

FIG. 1. Density-derived feature measurement in motor network. Motor network reconstruction (step 1). Extraction of GFA/MTR density-derived features along the M1-SMA intrahemispheric connection. Yellow arrows indicate the regions of interest (step 2). On the right, GFA/MTR histograms of M1-SMA for each control ($N = 10$) at tp1 and tp2; comparison of density-derived features between controls and patients at tp1–tp2. Each line is representing the significance of the p-value for each density-derived feature in each connection (intra- or interhemispheric). CC-m, corpus callosum-midline; GFA, generalized fractional anisotropy; M1, primary motor area; MTR, magnetization transfer ratio; PMd, premotor dorsal area; PMv, premotor ventral area; ROI, region of interest; N, total number of subjects; SC, somatosensory cortex; SMA, supplementary motor area.

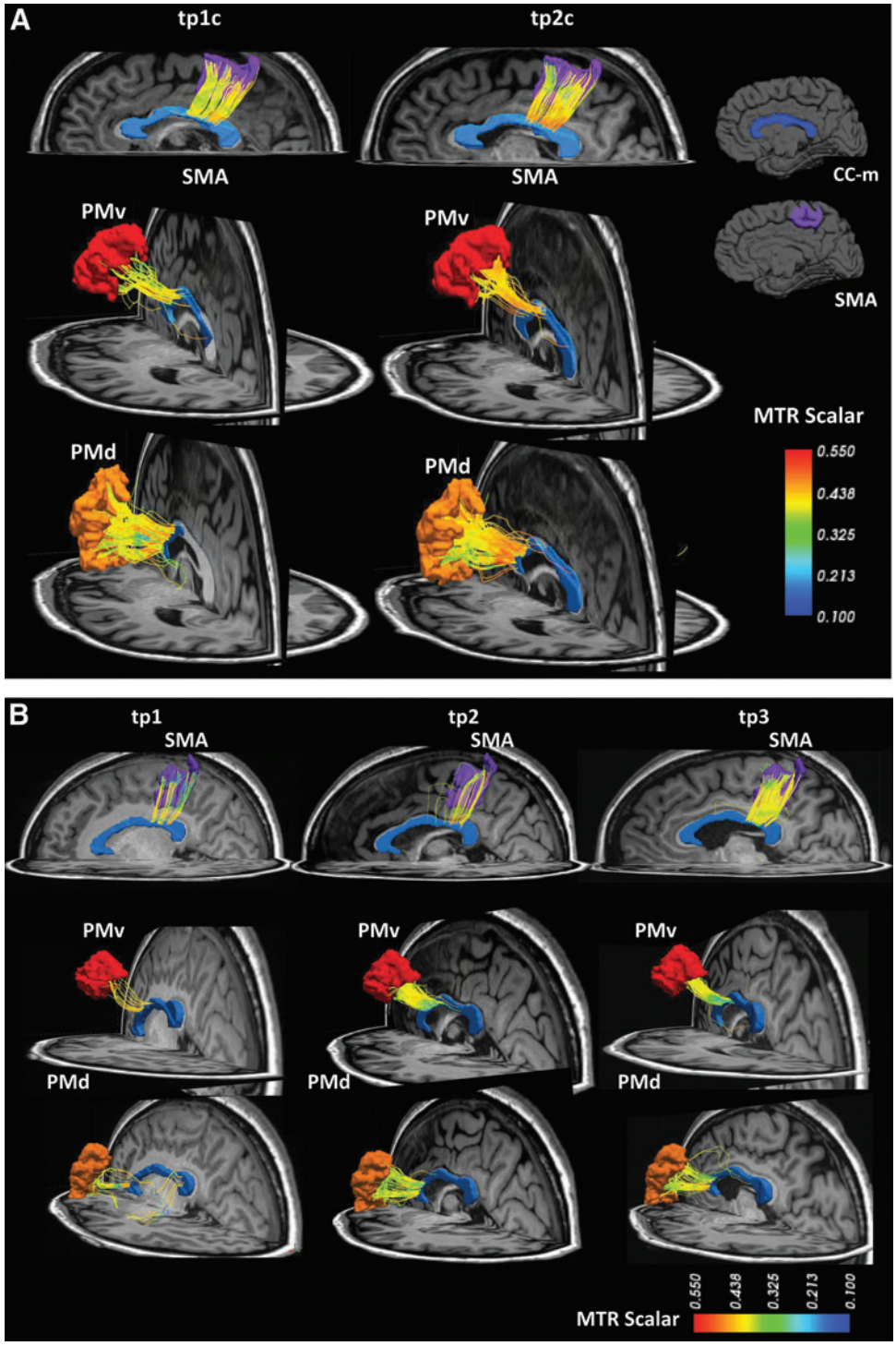

FIG. 2. DSI streamline tractography between SMA, PMv, and PMd and the CC-m in one control **(A)** and one patient **(B)**. MTR color scale (min. = 0.1, max. = 0.55). DSI, diffusion spectrum imaging.

Connectivity matrices were then obtained for each parameter, for both intra- and interhemispheric connections. Example of motor tracts is shown in Figure 2.

Statistical analysis

All statistics were performed using the R platform (www.r-project.org).

Stability in mean GFA/MTR mean values and density-derived features along motor tracts was assessed by evaluating statistical differences between tp1 and tp2 using a paired *t*-test (Supplementary Table S3). We then calculated percentage changes of mean and density-derived features between time points (Supplementary Table S4).

As parametric distribution of GFA/MTR mean and density-derived features was normal (Supplementary Tables S1 and S2; Supplementary Data are available online at www.liebertpub.com/brain), statistical analysis was performed using analysis of variance (ANOVA). The goal was to compare the following: (i) between patients and controls: changes in GFA/MTR mean values and density-derived features along motor tracts between time points 1 and 2; (ii) in patients:

Table 1. Patient Demographics and Stroke Characteristics

Patients	*Gender*	*Age at s/o*	*Stroke location*	*Artery involved*	*TOAST*
1	F	25	L Cortico-subcortical	L MCA	CE
2	M	66	L Subcortical	L MCA	LAA
3	F	39	R Cortico-subcortical	R MCA	CE
4	F	49	R Cortico-subcortical	R MCA	CE
5	M	76	L Subcortical	LMCA	CE
6	M	73	L Subcortical	L MCA L ACA	LAA
7	F	67	L Cortico-subcortical	L MCA	CE
8	M	62	R Cortico-subcortical	R MCA	LAA
9	M	35	R Cortico-subcortical	R MCA	LAA
10	M	69	R Cortico-subcortical	R MCA	LAA

s/o, Stroke onset; TOAST, Trial of Org 10172 in Acute Stroke Treatment (Ay et al., 2007); R MCA, right middle cerebral artery; L MCA, left middle cerebral artery; L ACA, left anterior cerebral artery; LAA, large artery atherosclerosis; and CE, cardio-aortic embolism.

changes across time points in GFA/MTR mean values and density-derived features along motor tracts.

Changes in mean GFA and MTR between time points were calculated as follows:

$$\Delta_{tp12}(\mathrm{M}) = |(\mathrm{M}_{tp2} - \mathrm{M}_{tp1})|/\mathrm{M}_{tp1},$$
$$\Delta_{tp13}(\mathrm{M}) = |(\mathrm{M}_{tp3} - \mathrm{M}_{tp1})|/\mathrm{M}_{tp1},$$
$$\text{and } \Delta_{tp23}(\mathrm{M}) = |(\mathrm{M}_{tp3} - \mathrm{M}_{tp2})|/\mathrm{M}_{tp2.}$$

Multivariate analysis of variance (MANOVA) was performed to assess the factors influencing MTR and GFA changes over time. We used GFA/MTR measures at all time points as dependent variables, and age, clinical scores at all time points (NIHSS motor, RANKIN, and FIM), and stroke sizes at tp3 as independent variables with two levels of factor: ''patients'' and ''controls'' for the first part of the analysis.

To assess the direction of changes in GFA/MTR mean values and density-derived features along motor tracts in patients compared with controls at tp12, we performed multiple *t*-test followed by multigroup comparison with false discovery rate (Benjamini and Hochberg, 1995). Results were illustrated by diagrams based on nodes and edges.

Correlation between GFA and MTR changes

Pearson's correlation was computed between changes in GFA/MTR mean/density-derived features at different time points (tp1–tp2, tp2–tp3, and tp1–tp3).

Biological interpretation of density-derived feature changes along WM tracts

In this work, we evaluated the temporal changes of three density-derived features (peak height, SD, and skewness) along the studied motor connections, both for GFA and MTR. There are currently no studies correlating the variation of these parameters to specific pathological changes in white matter microstructure. However, decreases in GFA/MTR peak height and skewness point theoretically to a comprehensive loss of general tract integrity (GFA) or of myelin (MTR) whereas an increase suggests sprouting/reconnection (GFA) or remyelination (MTR) phenomenon. SD appears to be less specific and more difficult to interpret biologically. Nevertheless, SD changes in either direction might be interpreted based on modifications of peak height and skewness in the same tract.

Results

Patients' demographics, clinical characteristics, and clinical scores are reported in Tables 1 and 2. In patients, the average stroke size was $58.6 \pm 74.6\,\mathrm{cm}^3$ (mean ± SD) at tp3.

Mean/density-derived feature analysis

GFA and MTR mean changes in the contralesional motor tracts were found in all patients at the three time points. Δ_{tp12}

Table 2. Patient Clinical Scores in the Acute Phase (Within 1 Week After Stroke), at 1-Month Follow-up and 6-Month Follow-up

	Acute			*1 Month*			*6 Months*		
Patients	*NIHSS* motor	*Rankin*	*FIM*	*NIHSS* motor	*Rankin*	*FIM*	*NIHSS* motor	*Rankin*	*FIM*
1	13	4	60	4	2	115	3	1	119
2	5	2	114	2	1	126	2	1	126
3	7	2	86	4	2	124	3	1	123
4	8	4	66	3	2	126	1	1	126
5	6	3	122	2	3	122	2	2	122
6	3	2	124	1	2	126	0	2	126
7	7	2	110	3	2	120	1	1	126
8	8	3	101	5	2	114	4	2	114
9	16	4	60	7	3	110	4	1	120
10	4	2	114	2	1	120	2	1	126

NIHSS motor, National Institutes of Health stroke motor score; FIM, functional independence measure.

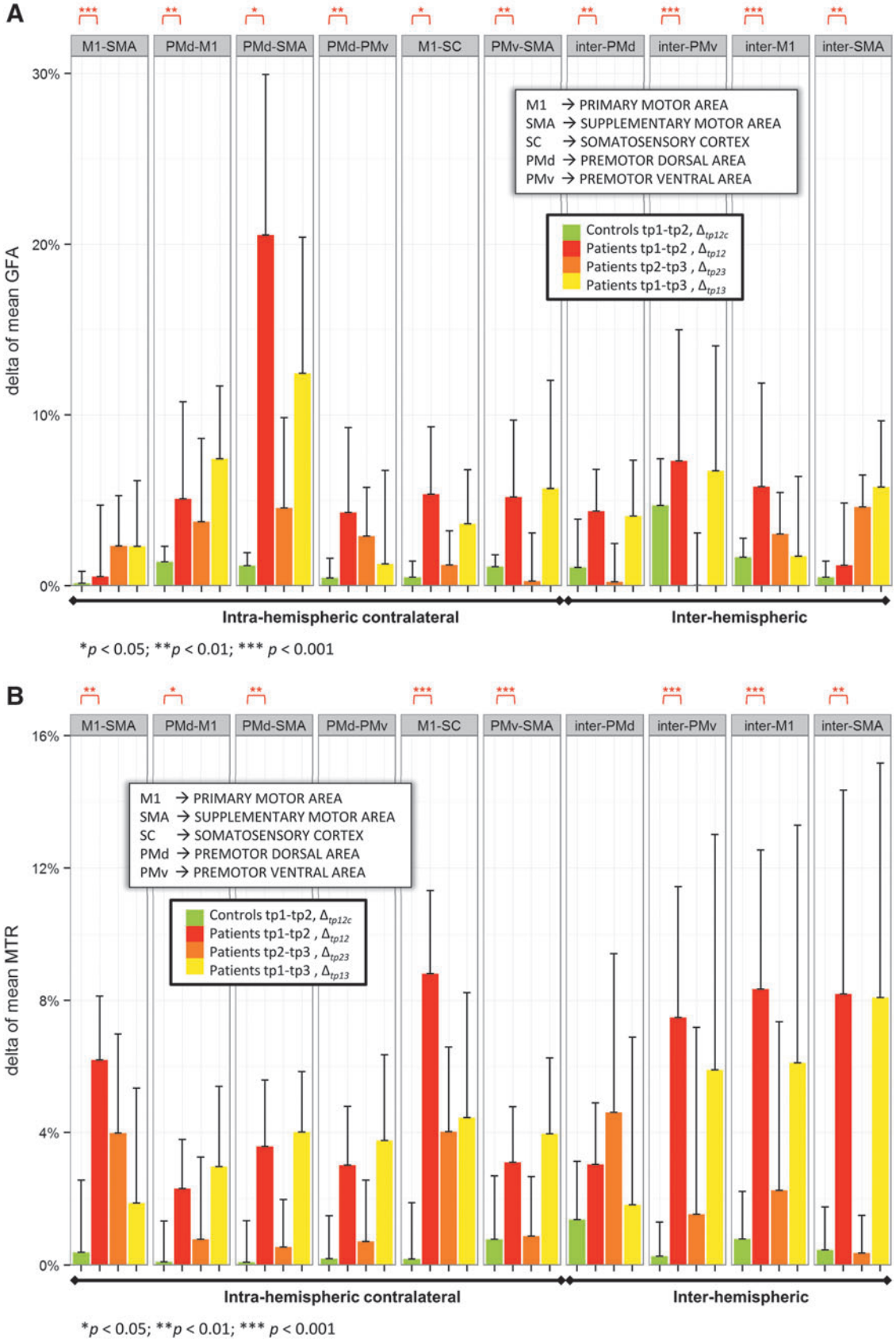

FIG. 3. Longitudinal changes of mean GFA **(A)** and mean MTR **(B)** in patients ($n = 10$) and controls ($n = 10$) (*$p < 0.05$, **$p < 0.01$, and ***$p < 0.001$).

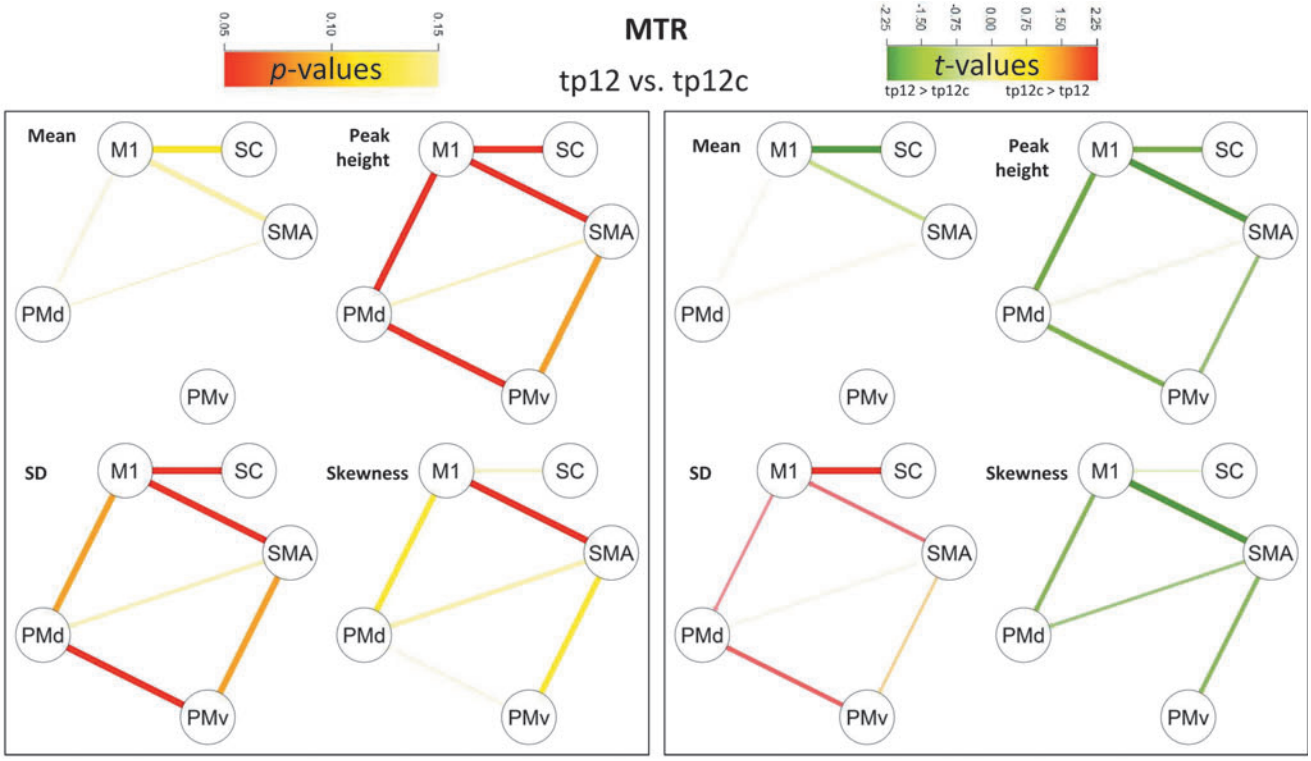

A Intra-hemispheric connections: adjusted-*p*-values **C** Intra-hemispheric connections: *t*-values

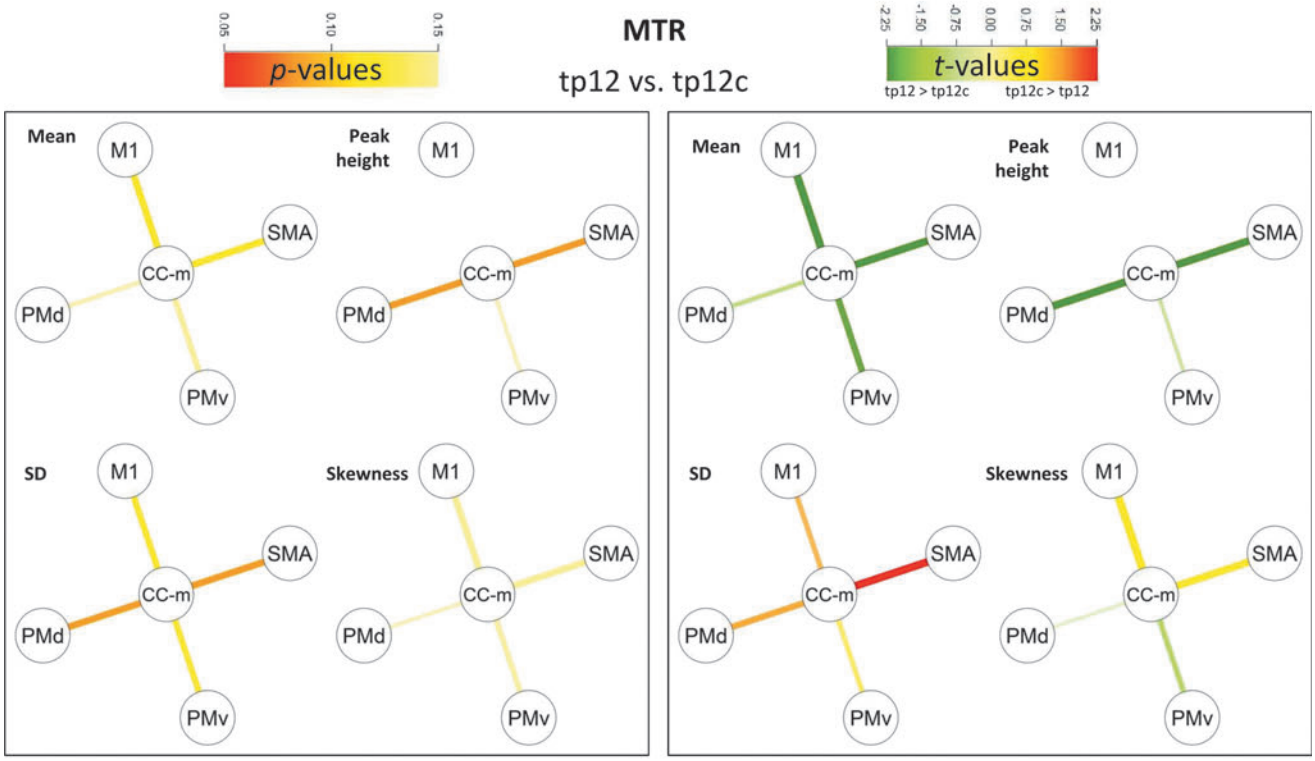

B Inter-hemispheric connections: adjusted-*p*-values **D** Inter-hemispheric connections: *t*-values

FIG. 4. Comparison of MTR mean and density-derived feature changes in patients and controls between tp2 and tp1 (tp12 vs. tp12c). M1 and SMA, PMv and PMd, and SC and CC-m. **(A)** Intra-hemispheric connections: adjusted *p*-values; **(B)** Inter-hemispheric connections: adjusted *p*-values; **(C)** Intra-hemispheric connections: *t*-values; **(D)** Inter-hemispheric connections: *t*-values.

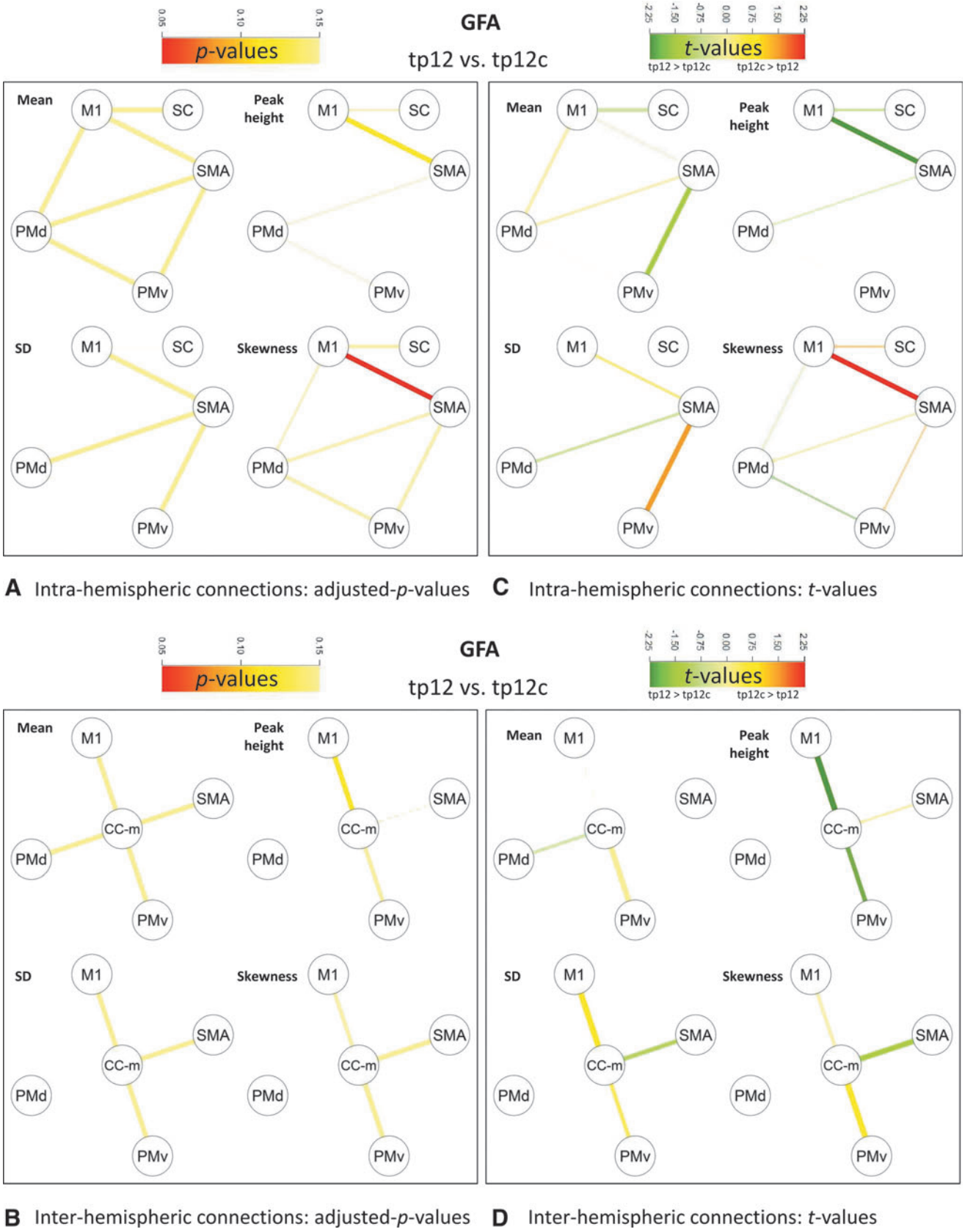

FIG. 5. Comparison of mean and GFA density-derived feature changes in patients and controls between tp2 and tp1 (tp12 vs. tp12c). M1 and SMA, PMv and PMd, and SC and CC-m. **(A)** Intra-hemispheric connections: adjusted *p*-values; **(B)** Inter-hemispheric connections: adjusted *p*-values; **(C)** Intra-hemispheric connections: *t*-values; **(D)** Inter-hemispheric connections: *t*-values.

Table 3. Multivariate Analysis of Variance of Mean MTR and Mean GFA as Dependent Factors and Age, Stroke Size, and Clinical Scores (NIHSS Motor, RANKIN, and FIM) as Independent Factors

		Intrahemispheric (residuals 22, df 6)				*Interhemispheric (residuals 22, df 4)*			
	Matrices	*MTR*		*GFA*		*MTR*		*GFA*	
Clinical score		F	p-*Value*	F	p-*Value*	F	p-*Value*	F	p-*Value*
Mean	AGE	5.326	0.003**	16.359	0.000***	0.865	0.503	2.494	0.077
	NIHSS motor	1.453	0.253	1.426	0.262	3.334	0.031*	7.423	0.001**
	STROKE SIZE	1.035	0.437	1.039	0.435	4.424	0.011*	9.632	0.000***
	RANKIN	0.432	0.847	0.665	0.679	2.806	0.055	2.629	0.067
	FIM	0.158	0.985	0.607	0.722	0.958	0.453	0.498	0.738

*$p<0.05$, **$p<0.01$, ***$p<0.001$.
GFA, generalized fractional anisotropy; MTR, magnetization transfer ratio.

Mean GFA and MTR differed significantly from Δ_{tp12c} mean GFA and MTR in almost all regions, with the exception of Δ_{tp12} mean MTR in PMd-PMv and inter-PMd connections (Fig. 3).

In controls, Δ_{tp12c} MTR in intra- and interhemispheric connections had a small negative correlation with GFA changes ($R^2=-0.0098$, $p=0.85$). In patients, Δ_{tp12}, Δ_{tp23}, and Δ_{tp13} in intra- and interhemispheric connections showed a positive significant correlation with GFA changes ($R^2=0.041$, $p=0.024$; $R^2=0.05$, $p=0.014$; $R^2=0.052$, $p=0.013$; see Supplementary Table S5 and Fig. S1).

Within 1 month after stroke, Δ_{tp12} MTR density-derived features along the intrahemispheric motor connections were significantly different from Δ_{tp12c} MTR density-derived features (Fig. 4A, C). Reduced peak height was observed for M1-SMA, M1-PMd, PMd-PMv, and M1-somatosensory cortex (SC) ($p<0.05$ corrected), as well as increased SD in M1-SMA, PMd-PMv, and M1-SC ($p<0.05$ corrected) and increased skewness in M1-SMA ($p<0.05$ corrected). As to group differences in GFA, Δ_{tp12} GFA density-derived features significantly differed from Δ_{tp12c} GFA density-derived features along the intrahemispheric M1-SMA connection (Fig. 5A, C), where increased skewness was observed ($p<0.05$ corrected).

No statistically significant dependence was observed between MTR- and GFA-derived feature changes.

Relationship between variations of MTR and GFA and clinical scores

Mean/density-derived feature GFA and MTR changes. MANOVA showed that between-group differences in mean GFA/MTR changes of intrahemispheric motor connections were dependent on age ($p<0.0001$ and $p<0.01$, respectively). As for interhemispheric connections, between-group differences in mean GFA changes were correlated with (i) NIHSS motor ($p<0.001$ and $p<0.05$), and (ii) stroke size ($p<0.001$ and $p<0.05$) (Table 3).

Table 4. Multivariate Analysis of Variance of MTR and GFA Density-Derived Features (Standard Deviation, Skewness, and Peak Height) as Dependent Factors and Age, Stroke Size, and Clinical Scores (NIHSS Motor, RANKIN, and FIM) as Independent Factors

		Intrahemispheric (residuals 22, df 6)				*Interhemispheric (residuals 22, df 4)*			
	Matrices	*MTR*		*GFA*		*MTR*		*GFA*	
Clinical score		F	p-*Value*	F	p-*Value*	F	p-*Value*	F	p-*Value*
SD	AGE	2.912	0.039*	2.094	0.108	0.305	0.871	10.520	0.000***
	NIHSS motor	3.499	0.019*	3.071	0.032*	1.425	0.264	2.623	0.067
	STROKE SIZE	1.462	0.249	1.415	0.266	1.468	0.251	0.917	0.474
	RANKIN	4.185	0.009**	1.007	0.453	0.907	0.480	1.828	0.165
	FIM	2.515	0.063	0.178	0.979	0.246	0.909	1.746	0.182
Skewness	AGE	0.408	0.864	1.827	0.153	0.449	0.772	1.092	0.389
	NIHSS motor	0.647	0.692	1.091	0.407	0.692	0.607	3.948	0.017*
	STROKE SIZE	3.000	0.035*	0.647	0.692	1.609	0.213	5.904	0.003**
	RANKIN	2.587	0.057	2.773	0.046*	0.977	0.443	4.452	0.010*
	FIM	0.711	0.646	1.584	0.212	0.107	0.979	5.767	0.003**
Peak height	AGE	0.827	0.565	2.385	0.074	2.375	0.089	6.333	0.002**
	NIHSS motor	1.429	0.261	0.872	0.535	0.651	0.634	0.908	0.479
	STROKE SIZE	1.344	0.292	1.458	0.251	3.222	0.035*	0.928	0.469
	RANKIN	0.991	0.462	0.217	0.966	1.063	0.402	1.532	0.233
	FIM	0.163	0.983	0.284	0.937	0.304	0.872	0.157	0.957

*$p<0.05$, **$p<0.01$, ***$p<0.001$.
SD, standard deviation.

As to MTR density-derived features, MANOVA evidenced that between-group differences in MTR SD changes of intrahemispheric motor connections were dependent on (i) age ($p < 0.05$), (ii) NIHSS motor ($p < 0.05$), and (iii) RANKIN ($p < 0.01$). Also, MTR skewness changes of intrahemispheric motor connections were highly dependent on stroke size ($p < 0.05$); the same dependency on stroke size of interhemispheric motor connections was observed for MTR peak height changes ($p < 0.05$) (Table 4).

Between-group differences in GFA SD changes of intrahemispheric motor connections were correlated with NIHSS motor ($p < 0.05$) and of interhemispheric motor connections were highly dependent on age ($p < 0.001$); GFA skewness changes of interhemispheric motor connections depended on (i) RANKIN scores ($p < 0.05$), (ii) NIHSS motor ($p < 0.05$), (iii) stroke size ($p < 0.01$), and (iv) FIM ($p < 0.01$). Also, peak height changes of interhemispheric motor connections depended on age ($p < 0.01$).

Discussion

This is the first study that uses tract-based measures and density-derived features (peak height, SD, and skewness) to assess myelin and axonal connectivity remodeling after stroke.

Our results show that both axonal remodeling and myelin remodeling occur in the contralesional motor network after stroke and provide evidence that GFA and MTR density-derived features improve the correlation with clinical scores in our cohort of patients, compared with mean values.

In a previous work, we revealed plastic changes in the contralateral motor network after stroke measured by mean GFA (Granziera et al., 2012b). GFA represents the standard deviation of diffusion directions in a single voxel and is described as the DSI (Q-ball) analogous of FA obtained in diffusion tensor experiments (Tuch, 2004). As to FA, therefore, GFA is supposed to be sensitive to axonal properties (integrity of the axonal membrane, myelin, as well as microtubule and microfilaments) and fiber density.

To disentangle the relative contribution of myelin and axonal remodeling in contralesional motor network remodeling, in the current work we investigated both GFA and MTR variations and their relationship. MTR is in fact a semiquantitative parameter that is sensitive to macromolecular presence and water content in the tissue and that highly depends on myelin contribution in white matter (Granziera et al., 2009, 2013a,b).

To reach this goal, we applied both mean and histogram tract-based analyses. In particular, histogram tract-based evaluation of GFA and MTR might better characterize connection properties than mean parametric values as they describe subtle parametric variations along a given trajectory, both cross-sectionally and longitudinally (Colby et al., 2012; Jones et al., 2005; Zhu et al., 2010, 2011).

Both mean/density-derived feature GFA and MTR changes were observed in the contralesional motor network within 1 month after stroke. These alterations were measured in almost all interhemispheric and intrahemispheric connections studied. Analysis revealed that GFA and MTR histograms had in general lower peak height, higher standard deviation, and variable skewness, suggesting a degeneration of both axonal and myelin components.

Interestingly, no correlations were found between GFA and MTR mean/density-derived feature changes at all time points, confirming the fact that, in our cohort of patients, these two measures are sensitive to different pathological phenomena. Future studies should aim to further investigate myelin contribution to GFA measures.

Both GFA and MTR mean values in the uninjured motor network well correlated with the NIHSS motor score whereas GFA and MTR density-derived features showed additional correlations with the RANKIN score, assessing patients' disability, and the FIM, another pure motor score. Together, therefore, mean and density-derived feature measures provided sensitive parameters that highly correlated with patients' clinical performance.

In conclusion, our study showed that both axonal remodeling and myelin remodeling occur in the contralesional motor network after stroke affecting motor regions. The combination of mean and density-derived feature tract-based analysis provided sensitive measures that highly correlate with patients' motor function and disability. A major limitation of the current study is that GFA and MTR are only indirect measures of axonal and myelin properties. Future studies should aim at analyzing more ''direct'' metric of white matter integrity, such as the one based on biophysical diffusion MRI models: AxCaliber (Assaf et al., 2008), ActiveAx (Alexander et al., 2010), and NODDI (Zhang et al., 2012). The studies should confirm and extend the current results in larger cohorts and different types of stroke.

Acknowledgments

The authors thank Centre d'Imagerie BioMédicale (CIBM) of the University of Lausanne, the Swiss Federal Institute of Technology Lausanne, the University of Genève, the Centre Hospitalier Universitaire Vaudois, the Hôpitaux Universitaires de Genève, the Leenaards, the Jeantet and the Stoicescu foundations; the Swiss National Science Foundation under grants PZ00P3_131914/11 and PP00P2-123438; the Swiss MS Society and the Societé Académique Vaudoise.

Author Disclosure Statement

Dr G. Krueger works for Siemens AG. Dr C. Granziera received travel fees and participates in advisory boards of Novartis, AG, Switzerland. Otherwise, no competing financial interests exist.

References

Alexander AL, Lee JE, Lazar M, Field AS. 2007. Diffusion tensor imaging of the brain. Neurotherapeutics 4:316–329.

Alexander DC, Hubbard PL, et al. 2010. Orientationally invariant indices of axon diameter and density from diffusion MRI. Neuroimage 52:1374–1389.

Assaf Y, Blumenfeld-Katzir T, Yovel Y, Basser PJ. 2008. AxCaliber: a method for measuring axon diameter distribution from diffusion MRI. Magn Reson Med 59:1347–1354.

Assaf Y, Pasternak O. 2008. Diffusion tensor imaging (DTI)-based white matter mapping in brain research: a review. J Mol Neurosci 34:51–61.

Ay H, Benner T, et al. 2007. A computerized algorithm for etiologic classification of ischemic stroke: the Causative Classification of Stroke System. Stroke 38:2979–2984.

Beaulieu C. The Biological Basis of Diffusion Tractography. In Proceedings of the Biomedical Imaging: Nano to Macro, 2006. 3rd IEEE International Symposium on 6–9 April 2006, p. 347.

Benjamini Y, Hochberg Y. 1995. Controlling the false discovery rate: a practical and powerful approach to multiple testing. J R Stat Soc Series B Stat Methodol 57:289–300.

Borich MR, MacKay AL, Vavasour IM, Rauscher A, Boyd LA. 2013. Evaluation of white matter myelin water fraction in chronic stroke. Neuroimage Clin 2:569–580.

Carmichael ST, Wei L, Rovainen CM, Woolsey TA. 2001. New patterns of intracortical projections after focal cortical stroke. Neurobiol Dis 8:910–922.

Chen JT, Collins DL, Freedman MS, Atkins HL, Arnold DL. 2005. Local magnetization transfer ratio signal inhomogeneity is related to subsequent change in MTR in lesions and normal-appearing white-matter of multiple sclerosis patients. Neuroimage 25:1272–1278.

Chollet F, DiPiero V, et al. 1991. The functional anatomy of motor recovery after stroke in humans: a study with positron emission tomography. Ann Neurol 29:63–71.

Colby JB, Soderberg L, et al. 2012. Along-tract statistics allow for enhanced tractography analysis. Neuroimage 59:3227–3242.

Crofts JJ, Higham DJ, et al. 2011. Network analysis detects changes in the contralesional hemisphere following stroke. Neuroimage 54:161–169.

Daducci A, Gerhard S, et al. 2012. The Connectome Mapper: an open-source processing pipeline to map connectomes with MRI. PLoS One 7:e48121.

Farrell JA, Zhang J, et al. 2010. Q-space and conventional diffusion imaging of axon and myelin damage in the rat spinal cord after axotomy. Magn Reson Med 63:1323–1335.

Gerhard S, Daducci A, et al. 2011. The connectome viewer toolkit: an open source framework to manage, analyze, and visualize connectomes. Front Neuroinform 5:3.

Gertheiss J, Goldsmith J, Crainiceanu C, Greven S. 2013. Longitudinal scalar-on-functions regression with application to tractography data. Biostatistics 14:447–461.

Granziera C, Ay H, Koniak SP, Krueger G, Sorensen AG. 2012a. Diffusion tensor imaging shows structural remodeling of stroke mirror region: results from a pilot study. Eur Neurol 67:370–376.

Granziera C, Daducci A, et al. 2012b. A new early and automated MRI-based predictor of motor improvement after stroke. Neurology 79:39–46.

Granziera C, Daducci A, et al. 2013a. Structural abnormalities in the thalamus of migraineurs with aura: a multiparametric study at 3 T. Hum Brain Mapp 35:1461.

Granziera C, D'Arceuil H, et al. 2007. Long-term monitoring of post-stroke plasticity after transient cerebral ischemia in mice using *in vivo* and *ex vivo* diffusion tensor MRI. Open Neuroimag J 1:10–17.

Granziera C, Romascano D, et al. 2013b. Migraineurs without aura show microstructural abnormalities in the cerebellum and frontal lobe. Cerebellum 12: 812–818.

Granziera C, Schmahmann JD, et al. 2009. Diffusion spectrum imaging shows the structural basis of functional cerebellar circuits in the human cerebellum *in vivo*. PLoS One 4:e5101.

Hagmann P, Kurant M, et al. 2007. Mapping human whole-brain structural networks with diffusion MRI. PLoS One 2:e597.

Helms G, Dathe H, Kallenberg K, Dechent P. 2008. High-resolution maps of magnetization transfer with inherent correction for RF inhomogeneity and T1 relaxation obtained from 3D FLASH MRI. Magn Reson Med 60:1396–1407.

Henkelman RM, Stanisz GJ, Graham SJ. 2001. Magnetization transfer in MRI: a review. NMR Biomed 14:57–64.

Jones DK, Travis AR, Eden G, Pierpaoli C, Basser PJ. 2005. PASTA: pointwise assessment of streamline tractography attributes. Magn Reson Med 53:1462–1467.

Jones TA, Kleim JA, Greenough WT. 1996. Synaptogenesis and dendritic growth in the cortex opposite unilateral sensorimotor cortex damage in adult rats: a quantitative electron microscopic examination. Brain Res 733:142–148.

Kinnunen KM, Greenwood R, et al. 2010. White matter damage and cognitive impairment after traumatic brain injury. Brain 134(Pt 2):449.

Lin YC, Daducci A, et al. Myelin Plasticity Does Not Significantly Influence Diffusion Remodelling of the Uninjured Motor Network After Stroke. In Proceedings of the 21th Annual Meeting of ISMRM, Salt Lake City, Utah, USA, 2013, p. 2934.

Luke LM, Allred RP, Jones TA. 2004. Unilateral ischemic sensorimotor cortical damage induces contralesional synaptogenesis and enhances skilled reaching with the ipsilateral forelimb in adult male rats. Synapse 54:187–199.

Mandl RC, Schnack HG, et al. 2010. Tract-based analysis of magnetization transfer ratio and diffusion tensor imaging of the frontal and frontotemporal connections in schizophrenia. Schizophr Bull 36:778–787.

Michel P, Odier C, et al. 2010. The Acute STroke Registry and Analysis of Lausanne (ASTRAL): design and baseline analysis of an ischemic stroke registry including acute multimodal imaging. Stroke 41:2491–2498.

Nossin-Manor R, Card D, et al. 2013. Quantitative MRI in the very preterm brain: assessing tissue organization and myelination using magnetization transfer, diffusion tensor and T(1) imaging. Neuroimage 64:505–516.

Ongur D, Du F. 2013. Probing myelin and axon abnormalities separately in psychiatric disorders using MRI techniques. Front Integr Neurosci 7:24.

Ozsunar Y, Grant PE, et al. 2004. Evolution of water diffusion and anisotropy in hyperacute stroke: significant correlation between fractional anisotropy and T2. AJNR Am J Neuroradiol 25:699–705.

Pierpaoli C, Basser PJ. 1996. Toward a quantitative assessment of diffusion anisotropy. Magn Reson Med 36:893–906.

Rehme AK, Fink GR, von Cramon DY, Grefkes C. 2011. The role of the contralesional motor cortex for motor recovery in the early days after stroke assessed with longitudinal FMRI. Cereb Cortex 21:756–768.

Riecker A, Groschel K, et al. 2010. The role of the unaffected hemisphere in motor recovery after stroke. Hum Brain Mapp 31:1017–1029.

Sled JG, Pike GB. 2001. Quantitative imaging of magnetization transfer exchange and relaxation properties *in vivo* using MRI. Magn Reson Med 46:923–931.

Song S-K, Sun S-W, et al. 2002. Dysmyelination revealed through MRI as increased radial (but unchanged axial) diffusion of water. Neuroimage 17:1429–1436.

Song S-K, Yoshino J, et al. 2005. Demyelination increases radial diffusivity in corpus callosum of mouse brain. Neuroimage 26:132–140.

Sotak CH. 2002. The role of diffusion tensor imaging in the evaluation of ischemic brain injury: a review. NMR Biomed 15:561–569.

Sun SW, Liang HF, et al. 2006. Noninvasive detection of cuprizone induced axonal damage and demyelination in the mouse corpus callosum. Magn Reson Med 55:302–308.

Takatsuru Y, Fukumoto D, et al. 2009. Neuronal circuit remodeling in the contralateral cortical hemisphere during functional recovery from cerebral infarction. J Neurosci 29: 10081–10086.

Tuch DS. 2004. Q-ball imaging. Magn Reson Med 52:1358–1372.

van den Heuvel MP, Mandl RC, Stam CJ, Kahn RS, Hulshoff Pol HE. 2010. Aberrant frontal and temporal complex network structure in schizophrenia: a graph theoretical analysis. J Neurosci 30:15915–15926.

Wang LE, Tittgemeyer M, et al. 2012. Degeneration of corpus callosum and recovery of motor function after stroke: a multimodal magnetic resonance imaging study. Human Brain Mapping 33:2941–2956.

Wedeen VJ, Hagmann P, Tseng WY, Reese TG, Weisskoff RM. 2005. Mapping complex tissue architecture with diffusion spectrum magnetic resonance imaging. Magn Reson Med 54:1377–1386.

Wedeen VJ, Wang RP, et al. 2008. Diffusion spectrum magnetic resonance imaging (DSI) tractography of crossing fibers. Neuroimage 41:1267–1277.

Weiller C, Chollet F, Friston KJ, Wise RJ, Frackowiak RS. 1992. Functional reorganization of the brain in recovery from striatocapsular infarction in man. Ann Neurol 31:463–472.

Weiller C, Ramsay SC, Wise RJ, Friston KJ, Frackowiak RS. 1993. Individual patterns of functional reorganization in the human cerebral cortex after capsular infarction. Ann Neurol 33:181–189.

Wheeler-Kingshott CA, Cercignani M. 2009. About ''axial'' and ''radial'' diffusivities. Magn Reson Med 61:1255–1260.

Zhang H, Schneider T, Wheeler-Kingshott CA, Alexander DC. 2012. NODDI: practical *in vivo* neurite orientation dispersion and density imaging of the human brain. Neuroimage 61:1000–1016.

Zhou LQ, Zhu YM, et al. 2004. A new method for analyzing histograms of brain magnetization transfer ratios: comparison with existing techniques. AJNR Am J Neuroradiol 25: 1234–1241.

Zhu H, Kong L, et al. 2011. FADTTS: functional analysis of diffusion tensor tract statistics. Neuroimage 56:1412–1425.

Zhu H, Styner M, et al. 2010. FRATS: Functional Regression Analysis of DTI Tract Statistics. IEEE Trans Med Imaging 29:1039–1049.

Address correspondence to:
Cristina Granziera
Laboratoire de Recherche en Neuroimagerie and Neuroimmunology Unit
Department of Clinical Neurosciences
Centre Hospitalier Universitaire Vaudois and University of Lausanne
Lausanne, VD
Switzerland

E-mail: cristina.granziera@chuv.ch